In situ high temperature x-ray diffraction measurements on a $(TiO_2)_{0.18}(SiO_2)_{0.82}$ xerogel using a curved image-plate

2000 J. Phys.: Condens. Matter 12 3521

(http://iopscience.iop.org/0953-8984/12/15/302)

J. Phys.: Condens. Matter **12** (2000) 3521–3529. Printed in the UK PII: S0953-8984(00)10465-5

In situ high temperature x-ray diffraction measurements on a $(TiO_2)_{0.18}(SiO_2)_{0.82}$ xerogel using a curved image-plate

D M Pickup†‖, G Mountjoy†, M A Roberts†‡, G W Wallidge†§, R J Newport† and M E Smith†§

† School of Physical Sciences, University of Kent at Canterbury, CT2 7NR, UK
‡ CLRC Daresbury Laboratory, Daresbury, Warrington, Cheshire WA4 4AD, UK
§ Department of Physics, University of Warwick, Coventry CV4 7AL, UK

Received 20 December 1999, in final form 9 February 2000

Abstract. *In situ* high temperature x-ray diffraction measurements have been performed on a $(TiO_2)_{0.18}(SiO_2)_{0.82}$ xerogel using a 185 mm radius curved image-plate. The results clearly show that the coordination of Ti in this material changes from predominantly sixfold to predominantly fourfold as the temperature is increased from 25 °C to 310 °C. An increase in the average O–O distance associated with this change is also identified. The use of the curved image-plate is shown to be a valuable technique for *in situ* studies of structural changes associated with thermal treatment of materials.

1. Introduction

Titania–silica mixed oxide materials, $(TiO_2)_x(SiO_2)_{1-x}$, are of significant technological importance. Silica glasses with a few mol% TiO_2 exhibit ultra-low thermal expansion [1] and mixed silicon–titanium oxides are important as catalysts and catalytic support materials [2]. In the optical industry they can be produced as anti-reflective thin films with tailored refractive indices [3]. The properties of titania–silica binaries are strongly dependent on their chemical composition, homogeneity and texture, which in turn depend on synthesis conditions. Homogeneity at the atomic level is especially important. Sol–gel synthesis, based on the hydrolysis and subsequent condensation of metal alkoxide precursors, provides a low temperature route to materials with a high level of atomic mixing and a high degree of porosity [1]. An important aspect of the sol–gel process is the transition from gel to glass during calcination. We have recently shown that for an unheated $(TiO_2)_{0.18}(SiO_2)_{0.82}$ xerogel, the titanium mostly occupies octahedral coordination with respect to oxygen: with heating to 750 °C the coordination of titanium converts to tetrahedral and can be considered as substituted within the silica network [4, 5]. Substitution of Ti into the silica network with heat treatment can be desirable in terms of the usefulness of these materials. For example, the catalytic activity and selectivity of silica rich $(TiO_2)_x(SiO_2)_{1-x}$ materials towards epoxidation of hexene has been attributed to the presence of Ti occupying tetrahedral sites within the silica network [6].

The curved image-plate technique developed by Finney and Bushnell-Wye provides a method for collecting x-ray diffraction data from amorphous materials in a fraction of the time required by conventional methods and hence allows scope for time-resolved experiments [7]. The image-plate technique involves the use of an arc-shaped camera with Debye–Scherrer

‖ Author to whom correspondence should be addressed.

0953-8984/00/153521+09$30.00

geometry in conjunction with an x-ray beam from a synchrotron radiation source. The camera, primarily constructed of aluminium and mounted on an optical bench exposed to the x-ray beam, holds an image-plate in an arc around the sample using a polycarbonate former (1 mm thick), thus allowing a significant portion of the Debye–Scherrer cones to be captured. Using a small arc, 185 mm, combined with short x-ray wavelength, data can be collected to high values of momentum transfer which, in turn, leads to the good real space resolution required to study amorphous materials. Simultaneous collection of the data over the whole angular range means collection times are of the order of minutes as opposed to the hours required by conventional incremental scanning.

In this paper, we describe the use of the curved image-plate technique to follow the structural changes within a $(TiO_2)_{0.18}(SiO_2)_{0.82}$ xerogel during calcination.

2. Experimental details: sample preparation

The sample was prepared using the following precursors: tetraethyl orthosilicate, TEOS, (Aldrich, 98%) and titanium (IV) isopropoxide, $Ti(OPr^i)_4$, (Aldrich, 97%). HCl was used as a catalyst to promote the hydrolysis and condensation reactions and isopropanol, IPA, (Fluka, 99.5%) was used as a mutual solvent. All reagents were loaded in a dry box and transferred using syringes to avoid absorption of moisture from the atmosphere. The dry box used was a single port type, connected to a vacuum pump and a cylinder of dry nitrogen. The alkoxide precursors were checked for hydrolysis using FTIR.

The preparation method used was that of Yoldas [8] which involves reacting $Ti(OPr^i)_4$ with a prehydrolysed solution of TEOS. The chosen prehydrolysis conditions were TEOS:IPA:H_2O in a 1:1:1 molar ratio in the presence of HCl (pH 1), stirring for two hours. The resulting sol was stirred for a few minutes before water was added slowly such that the overall water:alkoxide molar ratio (R) was 2. Stirring was continued until the sol had gelled which took two days. The gel was air dried for several days, finely ground and then pumped under vacuum for 24 hours to remove any excess solvent.

It is well known that sol–gel-derived materials usually contain residual organic fragments, e.g. unreacted alkoxide groups, which are gradually lost during calcination. Since the sample composition needs to be known for the analysis of the x-ray diffraction data, it was estimated at various temperatures using the following method. Firstly, the Ti:Si ratio in the final xerogel was assumed to be the same as that of the sol. The total M:O ratio (M = Ti and Si) was estimated using ^{29}Si MAS NMR which yields the distribution of Q^n species present in the network structure (Q^n stands for an SiO_4 unit with n bridging oxygens [9]). Finally, the carbon and hydrogen, and total oxygen content were estimated from TGA (thermogravimetric analysis) results, assuming that the weight loss was predominantly due to the loss of ethanol and isopropanol. Estimates of the sample composition at various temperatures are shown in table 1.

Table 1. Estimates of total composition and density of the $(TiO_2)_{0.18}(SiO_2)_{0.82}$ xerogel at various temperatures.

Temperature (°C)	Composition (at.%)					Density (g cm^{-3})
	% Ti	% Si	% O	% C	% H	
25	2.3	10.4	29.0	16.3	42.1	1.86
210	5.4	24.8	68.3	0.4	1.1	1.89
310	5.6	25.5	68.8	0	0	1.90
500	5.8	26.5	67.7	0	0	1.93

Estimates of the density of the sample at various temperatures were also required in the analysis of the x-ray data. To this end, the density of the unheated xerogel and a portion of the sample preheated to 750 °C were measured using the Archimedes method with 2-butanol as the liquid of known density ($\rho = 0.808$ g cm^{-3}). The densities of the sample at other temperatures were estimated by interpolation and these results are also presented in table 1.

3. Experimental details: x-ray diffraction

The x-ray diffraction data were collected on station 9.1 at the Daresbury Laboratory SRS using a 185 mm radius camera fitted with a 400×148 mm^2 image-plate (Fuji Bass IIIs). The wavelength was set at $\lambda = 0.4868$ Å, and calibrated using the K edge of an Ag foil; this value was low enough to provide data to a high value of momentum transfer ($\sim$21 Å^{-1}) and to reduce the effects of fluorescence from the titanium present in the sample. The sample was contained in a 1 mm diameter silica capillary and mounted at the centre of curvature of the image-plate. Heating under an ambient atmosphere was provided by a custom-made furnace fitted with polyimide windows. Calibration of the furnace revealed the temperature controller to be accurate to within ± 10 °C.

Data were collected at room temperature, 85 °C, and then at intervals of $\sim$50 °C up to 500 °C. Each temperature was maintained for 10 min before data collection commenced. The data collection time was 45 min per image. Each stored image was scanned within 10 min from the image-plate using a Molecular Dynamics scanner to avoid significant degradation of the image from self-decay processes. Calibration of the data were achieved by using a 'grid calibration' technique to convert the pixel positions from the image-plate into distance measurements from which the 2θ angles could be determined on the basis of camera geometry and the use of a silicon calibration standard [7]. Data were also collected from the empty capillary tube and empty furnace for background subtraction purposes.

4. Results and data analysis

The preliminary analysis of the x-ray diffraction data involved integration of the Debye–Scherrer cones recorded by the image-plate, a correction for incident x-ray beam polarization and background subtraction. Next, corrections were made to the scattered x-ray intensity in order to account for absorption of the incident x-ray beam by the sample and for inelastic scattering, or Compton scattering. No correction was made to account for multiple scattering since it is generally accepted that it can be neglected in x-ray diffraction because of relatively low intensities. For this experiment, the sample geometry was such that the absorption correction had negligible angular variation [10] and could be included in the data scaling factor. The data scaling factor is required because the experimental x-ray data are not measured in electron units; its effect is to normalize the data such that it oscillates about the self-scattering term. This type of normalization is known as the high angle method. For these data, the self-scattering and Compton scattering were calculated from tables [11, 12] using the composition data presented in table 1. Any small residual background was subtracted from the data using a polynomial.

For an amorphous material with no preferred orientation, spherical symmetry of the electron density can be assumed and the x-ray diffraction can be described by:

$$I_{eu} = N \sum_{i=1}^{T} c_i f_i^2 + N \sum_{i=1}^{T} \sum_{j=1}^{T} c_i f_i c_j f_j \int_0^{\infty} r d_{ij}(r) \frac{\sin Qr}{Qr} \, \mathrm{d}r$$

where there are T different elements and i and j each represent different elements. The atomic scattering factors or form factors for elements i and j are f_i and f_j, respectively. The quantities c_i and c_j are the fractional concentrations of elements i and j, respectively, and N is the total number of atoms in the sample. The quantity involving the f_i^2 term is known as the self-scattering. The differential pair correlation function, $d_{ij}(r)$, is given by:

$$d_{ij}(r) = 4\pi r(\rho_{ij}(r) - \rho_0)$$

where $\rho_{ij}(r)$ represents the number of type j atoms per unit volume of sample at a distance r away from type i atoms and ρ_0 is the average of this function. The structure factor, $S(Q)$, can be obtained by subtracting the self-scattering term from the scattered intensity. The form factors can be simplified by defining an average scattering factor per electron [13]:

$$f_e = \left(\sum_i c_i f_i\right)\left(\sum_i c_i Z_i\right)^{-1}$$

where the sum over i represents the weighted sum over the atoms of atomic number Z_i. The form factor for each element can then be approximated by $f_i = K_i f_e$, where K_i will be approximately equal to Z_i. In each case, K_i will vary with the scattering vector $\boldsymbol{Q}$, and the validity of this treatment depends on the error in treating K_i as an average over the entire $\boldsymbol{Q}$-range involved.

Defining the interference function, $i(Q)$, and inverting by Fourier transformation yields the total $d(r)$:

$$i(Q) = \left(I_{eu} - N\sum_i c_i f_i^2\right)\left(\sum_i c_i f_i^2\right)^{-2}$$

$$d(r) = \frac{2}{\pi}\int_0^\infty Qi(Q)M(Q)\sin Qr\,\mathrm{d}Q$$

where $M(Q)$ is a modification function which is zero for $Q \geqslant Q_{max}$ and is required to reduce the truncation effects associated with the finite range of Q over which the experiment is performed. However, structural parameters were obtained from the x-ray data presented here by generating fits to the data in Q-space and comparing the experimental and calculated results in r-space, thereby reducing the problems associated with direct transformation methods. Atomic correlations were generated in Q-space using the following equation [14]:

$$i(Q)_{ij} = \frac{N_{ij}\omega_{ij}}{c_j}\frac{\sin QR_{ij}}{QR_{ij}}\exp\left[\frac{-Q^2\sigma_{ij}^2}{2}\right]$$

where i and j are the elements in the correlation being modelled, ω_{ij} is the x-ray weighting factor associated with the correlation, N_{ij} is the average coordination number of atoms j around i, R_{ij} is the average distance between i and j and σ_{ij} is the standard deviation of the distribution of R_{ij}. σ_{ij} is related to the Debye–Waller factor (A) by $A = 2\sigma_{ij}^2$.

The x-ray weighting factor, ω_{ij}, is defined by:

$$\omega_{ij} = \frac{(2 - \delta_{ij})c_i c_j Z_i Z_j}{[\bar{Z}]^2}$$

where δ_{ij} is a Kronecker delta function.

Four correlations were used in the modelling procedure: an Si–O distance of ~1.6 Å, a Ti–O distance of 1.8–2.0 Å, an O–O distance of ~2.6 Å and an M–M (M = Si or Ti) distance of ~3.1 Å. Values of R_{ij}, N_{ij} and σ_{ij} were estimated for each correlation and a calculated $i(Q)$ generated. The goodness of fit was judged by Fourier transforming both the data and the fit and comparing the peaks in the real space correlation functions. The Fourier transforms

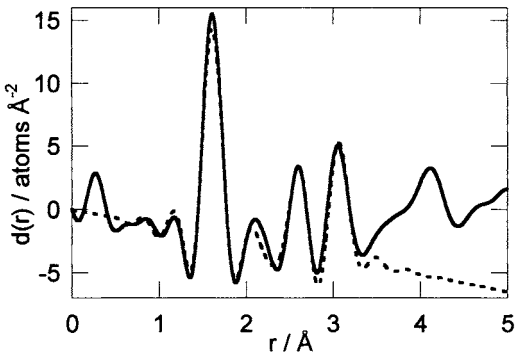

Figure 1. Experimental (solid line) and calculated (dotted line) differential correlation functions, $d(r)$, for an SiO_2 capillary.

Table 2. Structural parameters for the SiO_2 capillary obtained from modelling of the x-ray data. Note that the errors are ±0.02 Å in R, ±10% in N and ±20% in A.

Temp. (°C)	25
N_{Si-O}	4.3
R_{Si-O} (Å)	1.61
A_{Si-O} (Å^2)	0.002
N_{O-O}	5.5
R_{O-O} (Å)	2.60
A_{O-O} (Å^2)	0.005
N_{Si-Si}	4.0
R_{Si-Si} (Å)	3.04
A_{Si-Si} (Å^2)	0.01

were carried out over the Q-range 0.7–21.1 Å^{-1} using a Hanning window function [15] to reduce termination ripples. The structural parameters (R, N and σ) were then varied and the process repeated until satisfactory agreement between the experimental and calculated real space correlation functions was obtained. It should be noted that the purpose of fitting the real space peak at ∼3.1 Å was to account for any contribution it may have to the O–O peak. Since this peak may include contributions from correlations involving Ti, obtaining reliable information about the Si–Si correlations would be difficult.

Since x-ray diffraction data were collected from both the empty SiO_2 capillary and the empty furnace, it was possible to analyse the data from the capillary and obtain structural parameters. Amorphous SiO_2 has been well studied using x-ray and neutron diffraction, and hence the data from the capillary allowed us to check the validity of our data collection and analysis. The results obtained from the SiO_2 capillary are shown in table 2; table 3 contains some results from the literature for comparison [16]. Figure 1 shows a comparison of the experimental and calculated differential correlation functions for the SiO_2 capillary. Good agreement is displayed between the results from the capillary and those in the literature from amorphous silica.

The structural parameters obtained *in situ* at various temperatures from the $(TiO_2)_{0.18}(SiO_2)_{0.82}$ xerogel are shown in table 4. Figures 2 and 3 show the real space fits to the x-ray data collected at 25 °C and 500 °C. There is some discrepancy between the data and the calculated fits in the region 2.0–2.5 Å; this discrepancy is probably due to Si–H correlations

Table 3. Structural parameters for amorphous silica obtained from neutron diffraction data [16].

	25 °C	682 °C	1036 °C
N_{Si-O}	3.85	3.67	3.62
R_{Si-O} (Å)	1.62	1.63	1.63
A_{Si-O} (Å^2)	0.004	0.007	0.009
N_{O-O}	5.68	5.23	5.04
R_{O-O} (Å)	2.65	2.65	2.65
A_{O-O} (Å^2)	0.014	0.029	0.036

Table 4. *In situ* structural parameters for $(TiO_2)_{0.18}(SiO_2)_{0.82}$ xerogel at various temperatures obtained from modelling of x-ray diffraction data. Note that the errors are ±0.02 Å in R, ±10% in N and ±20% in A.

	25 °C	210 °C	310 °C	500 °C
N_{Si-O}	4.4	4.4	4.3	4.2
R_{Si-O} (Å)	1.62	1.63	1.62	1.62
A_{Si-O} (Å^2)	0.002	0.007	0.004	0.010
N_{Ti-O}	6.0	4.8	4.0	4.0
R_{Ti-O} (Å)	1.97	1.98	1.82	1.82
A_{Ti-O} (Å^2)	0.005	0.034	0.005	0.007
N_{O-O}	5.3	4.6	4.6	5.0
R_{O-O} (Å)	2.62	2.63	2.69	2.73
A_{O-O} (Å^2)	0.02	0.034	0.051	0.045
N_{M-M}	6.8	5.8	5.9	4.3
R_{M-M} (Å)	3.09	3.08	3.12	3.09
A_{M-M} (Å^2)	0.045	0.039	0.051	0.024

in the experimental data arising from the presence of Si–OH groups in the sample. The Si–O–H bond angle is typically 122° and Si–H distances are in the range 2.0–2.4 Å [17]. The Si–H correlations have not been modelled here because of their small contribution relative to the Si–O and Si–OH correlations.

The errors quoted in table 4 are estimates of the statistical uncertainties associated with the fitting process. Roberts *et al* [7] have previously shown, by comparison with results from conventional scanning, that the systematic errors associated with the use of the curved image-plate technique are not significant.

5. Discussion

The structural parameters obtained from the fitting of the x-ray diffraction data in table 4 clearly show the average Ti–O coordination number changing from ∼6 to ∼4 between the temperatures of 25 °C and 310 °C. This structural change is confirmed by the average Ti–O distance shortening from 1.98 Å to 1.82 Å between 25 °C and 310 °C; the distance of 1.98 Å is close to that found in TiO_2 (anatase or rutile) where Ti is octahedrally coordinated [18] and the distance of 1.82 Å compares well with that found in TS-1 (a zeolite from the pentasil family containing a few mol% of Ti) where Ti is known to substitute directly for Si in tetrahedral sites [19]. The change in Ti local environment probably occurs by two mechanisms. One is the substitution of TiO_4 groups into the silica network with heat treatment and the other is the reversible loss of H_2O from some sixfold Ti sites. The latter reversible mechanism has recently been identified in this type of material using *in situ* XANES measurements [20]. The results

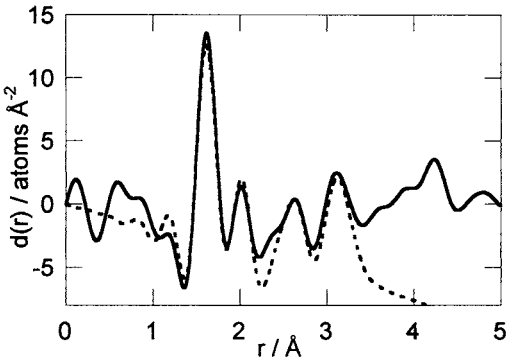

Figure 2. Experimental (solid line) and calculated (dotted line) differential correlation functions, $d(r)$, for the $(TiO_2)_{0.18}(SiO_2)_{0.82}$ xerogel at 25 °C.

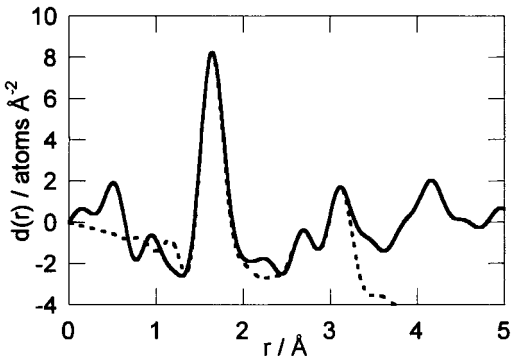

Figure 3. Experimental (solid line) and calculated (dotted line) differential correlation functions, $d(r)$, for the $(TiO_2)_{0.18}(SiO_2)_{0.82}$ xerogel heated *in situ* to 500 °C.

show very little change in the Ti–O correlation on heating from 310 °C to 500 °C indicating that the Ti is stable within the silica network up to 500 °C. Examining the differential correlation functions, one can see that the peak at ∼1.6 Å is much broader by 310 °C, illustrating that by this temperature the correlation includes a significant contribution from the short Ti–O distance. In contrast, for the room temperature data the Ti–O correlation appears as a separate peak.

At 210 °C, significant proportions of both four- and sixfold coordinated Ti are present; this is illustrated by the high Debye–Waller factors for the correlation shells notionally assigned to Si–O and Ti–O, and by the intermediate Ti–O coordination number. The Ti–O distance at 210 °C of 1.98 Å represents only the contribution from the sixfold Ti with the fourfold Ti contributing to the peak assigned to Si–O and resulting in a large Debye–Waller factor for that peak. Modelling the data collected at 210 °C with a combination of four- and sixfold Ti would involve the introduction of three more fitting parameters which, in this case, may reduce confidence in the degree of uniqueness of the resultant model.

The results in table 4 also yield information on the effect that heat treatment and Ti substitution has on the silica network. The parameters for the Si–O correlation are close to those in table 3 for pure silica, showing that Si remains in SiO_4 tetrahedra as expected. The increase in the Debye–Waller factor for this correlation between 25 °C and 500 °C is in part

due to an increase in thermal disorder as the temperature is raised (the high Debye–Waller factor for the Si–O correlation at 210 °C being also due to a contribution to this peak from some fourfold Ti). The O–O distance exhibits very different behaviour in pure silica compared to the $(TiO_2)_{0.18}(SiO_2)_{0.82}$ xerogel; in silica it is constant up to 1036 °C where as in the xerogel it increases by ∼0.1 Å at 500 °C. This increase is most likely due to Ti substituting into the silica network, since the average O–O distance in a TiO_4 tetrahedron is greater than that in an SiO_4 tetrahedron. For a regular TiO_4 tetrahedron the O–O distance is 2.97 Å whereas for the SiO_2 counterpart it is 2.64 Å. Consequently, a $(TiO_2)_{0.18}(SiO_2)_{0.82}$ sample where all the Ti is substituted within the silica network would be expected to have an average O–O distance of 2.70 Å. This calculated distance agrees well with our experimental results confirming that most of the Ti is substituted into the silica network at 500 °C. The O–O coordination numbers for the xerogel are all close to five and reflect incomplete condensation of the network structure at these temperatures (a fully condensed tetrahedral network structure would have an O–O coordination number of 6). This observation agrees with FTIR and ^{29}Si MAS NMR results from preheated $(TiO_2)_x(SiO_2)_{1-x}$ xerogels [21] which indicate the presence of non-bridging hydroxy groups.

6. Conclusions

The curved image-plate technique has been used to follow structural changes within a $(TiO_2)_{0.18}(SiO_2)_{0.82}$ xerogel during calcination. The results clearly show that the coordination of Ti changes from predominantly sixfold to predominantly fourfold as the temperature is increased from 25 °C to 310 °C. An increase in the average O–O distance associated with this change has also been identified. The results are consistent with those of previous EXAFS and XANES studies on such materials [4, 5]. The curved image-plate technique has proved to be a valuable tool for collecting *in situ* high temperature x-ray diffraction data on amorphous materials over a large Q-range in a single exposure and for monitoring structural changes in a time-resolved fashion.

Acknowledgments

The EPSRC is thanked for its support through various grants. W A Steer is thanked for his help with the data collection and analysis.

References

[1] Brinker C J and Scherrer G W 1990 *Sol–Gel Science: the Physics and Chemistry of Sol–Gel Processing* (San Diego, CA: Academic)
[2] Itoh M, Hattori H and Tanabe K J 1974 *J. Catal.* **35** 225
[3] Schultz P C and Smyth H T 1972 *Amorphous Materials* ed E W Douglas and B Ellis (London: Wiley)
[4] Anderson R, Mountjoy G, Smith M E and Newport R J 1998 *J. Non-Cryst. Solids* **232–234** 72
[5] Mountjoy G, Pickup D M, Wallidge G W, Anderson R, Cole J M, Newport R J and Smith M E 1999 *Chem. Mater.* **11** 1253
[6] Davis R J and Lui Z 1997 *Chem. Mater.* **9** 2311
[7] Roberts M A, Finney J L and Bushnell-Wye G 1998 *Mater. Sci. Forum* **278–281** 318
[8] Yoldas B E 1980 *J. Non-Cryst. Solids* **38** 81
[9] Engelhardt G and Michel D 1987 *High Resolution Solid State NMR of Silicates and Zeolites* (Chichester: Wiley)
[10] Bond W L 1972 *International Tables for X-ray Crystallography* vol II (Birmingham: Kynoch) p 291
[11] 1974 *International Tables for X-ray Crystallography* vol IV (Birmingham: Kynoch) p 71
[12] Hajdu F 1972 *Acta. Crystallogr.* A **28** 250
[13] Warren B E 1990 *X-ray Diffraction* (New York: Dover)

[14] Gaskell P H 1991 *Glasses and Amorphous Materials (Material Science and Technology 9)* ed J Zarzycky (Weinheim: VCH) p 175
[15] Press W H, Flannery B P, Teukolsky S A and Vetterling W T 1986 *Numerical Recipes: The Art of Scientific Computing* (Cambridge: Cambridge University Press)
[16] Susman S, Volin K J, Montague D G and Price D L 1991 *Phys. Rev.* B **43** 11 076
[17] Fletcher D A, McMeeking R F and Parkin D 1996 *J. Chem. Inf. Comput. Sci.* **36** 746
[18] Huggins M L 1926 *Phys. Rev.* **27** 638
[19] Vayssilov G N 1997 *Catal. Rev. Sci. Eng.* **93** 209
[20] Mountjoy G, Pickup D M, Wallidge G W, Cole J M, Newport R J and Smith M E 1999 *Chem. Phys. Lett.* **304** 150
[21] Pickup D M, Mountjoy G, Wallidge G W, Anderson R, Cole J M, Newport R J and Smith M E 1999 *J. Mater. Chem.* **9** 1299